

A fully coupled thermo-mechanical analysis for the minimisation of spring-in and process time in ultra-thick components for wind turbine blades

Struzziero, G.; Teuwen, J. J.E.

DOI

[10.1016/j.compositesa.2020.106105](https://doi.org/10.1016/j.compositesa.2020.106105)

Publication date

2020

Document Version

Final published version

Published in

Composites Part A: Applied Science and Manufacturing

Citation (APA)

Struzziero, G., & Teuwen, J. J. E. (2020). A fully coupled thermo-mechanical analysis for the minimisation of spring-in and process time in ultra-thick components for wind turbine blades. *Composites Part A: Applied Science and Manufacturing*, 139, Article 106105. <https://doi.org/10.1016/j.compositesa.2020.106105>

Important note

To cite this publication, please use the final published version (if applicable). Please check the document version above.

Copyright

Other than for strictly personal use, it is not permitted to download, forward or distribute the text or part of it, without the consent of the author(s) and/or copyright holder(s), unless the work is under an open content license such as Creative Commons.

Takedown policy

Please contact us and provide details if you believe this document breaches copyrights. We will remove access to the work immediately and investigate your claim.



A fully coupled thermo-mechanical analysis for the minimisation of spring-in and process time in ultra-thick components for wind turbine blades

G. Struzziero, J.J.E. Teuwen

Faculty of Aerospace, Aerospace Manufacturing Technologies, Delft University of Technology, Delft 2628 CD, Netherlands

ARTICLE INFO

Keywords:

- A. Thermosetting resin
- B. Cure behaviour
- C. Numerical analysis
- E. Vacuum infusion

ABSTRACT

The paper tackles the multi-objective optimisation of the cure stage of the Vacuum Assisted Resin Transfer Moulding (VARTM) process to manufacture the root insert of wind turbine blades. The aim of the study is to compare the Pareto front obtained from a pure heat transfer analysis, where temperature overshoot is an objective, with the one achieved when a coupled thermo-mechanical analysis is used, in which spring-in deflection is directly addressed. The optimisation methodology links the finite element solution of a heat transfer and a coupled thermo-mechanical problem of the cure process with a genetic algorithm suitable for multi-objective problems. The paper highlights that whilst minimising overshoot temperature is effective in reducing the spring-in, optimal design points might remain hidden. Furthermore, by showing the evolution of transverse residual stresses the paper suggests that designing cure cycles that introduce compressive stresses before vitrification is beneficial to counteract the subsequent tensile stresses generation.

1. Introduction

The urgency of climate change and consequent need to reduce greenhouse gas emissions is pushing our society towards an energy transition from fossil fuels-based sources to renewable energy sources such as wind energy. Within this context, maximising the efficiency of the wind turbine blade manufacturing is a crucial step towards this transition. Due to the higher mechanical performance per weight compared to standard materials (i.e. aluminium alloys, steel) the use of composite materials has already positively contributed to the reduction of CO₂, however the extraction of the materials involved is in itself contributing to the emission of CO₂. Moreover, the electricity consumed by the manufacturing process has been most likely generated by burning fossil fuels. Therefore, a sustainable composite manufacturing practice can reduce emissions of the final product mostly by (I) wasting as little material as possible (II) minimising number of processes (i.e. minimising energy consumption), temperature and their duration (III) minimising process-induced defects and expanding life span of the part [1,2]. To achieve a sustainable manufacturing practice the three factors have to be met for each newly produced part.

The manufacturing of the root insert of a wind turbine blade is achieved via Vacuum Assisted Resin Transfer Moulding (VARTM). Due to the high thicknesses involved (i.e. 100 mm) the process is highly challenging and several defects can be introduced during the impregnation stage of the process (i.e. dry spots, voids) and during the curing

stage (i.e. spring-in after removal, matrix cracking); the occurrence of the aforementioned defects can lead to rejection of the part. In the last two decades a significant research effort has been performed in the context of optimisation of composite manufacturing processes such as Liquid Composite Moulding (LCM), pultrusion, autoclave tackling draping, impregnation and cure stage [3]. Concerning the cure stage, from the early works on single objective optimisation to minimise cost related [4,5], and quality related objectives [6–10] researchers have moved towards weighted fitness function minimisation [11,12] to account for more than one objective. Part distortion due to cure-induced defects has only been addressed by optimisation of mould angles to compensate the demoulded part distortion [10]. However, it is only via multi-objective (MO) optimisation set-ups that the three aforementioned factors can be addressed simultaneously. As pointed out in [3] MO optimisation constitutes the way forward to address the challenges within composite manufacturing by discovering new optimal design opportunities in terms of cost and quality. The MO optimisation of the cure stage of batch processes has been also undertaken considering overshoot temperature and cure time as objectives [13] and cure time and degree of cure gradients [14,15]. The results highlighted that Manufacturer Recommended Cure Cycles (MRCC) do not provide optimal solutions and that via quantifying the Pareto front of the problem significant reduction in the addressed objectives can be obtained. The objectives addressed in literature are related to (1) cost reduction and energy saving (i.e. cure time), (2) maximising quality (i.e. minimising

E-mail addresses: G.Struzziero@tudelft.nl (G. Struzziero), J.J.E.Teuwen@tudelft.nl (J.J.E. Teuwen).

<https://doi.org/10.1016/j.compositesa.2020.106105>

Received 6 July 2020; Received in revised form 7 August 2020; Accepted 30 August 2020

Available online 09 September 2020

1359-835X/ © 2020 The Author(s). Published by Elsevier Ltd. This is an open access article under the CC BY license (<http://creativecommons.org/licenses/by/4.0/>).

gradients in both temperature and degree of cure, residual stresses and by avoiding reaching temperature degradation). So far, the MO optimisation of the cure stage of the VARTM process has been addressed by only implementing heat transfer analysis solution and by using overshoot temperature as a metric to reduce residual stresses generation [6,13,16,17]. When a thermo-mechanical coupled analysis was implemented, the problem has only been addressed by using Single Objective (SO) optimisation [3]. Furthermore, the effectiveness of using overshoot temperature as a metric to reduce residual stresses has not been tackled yet. The aim of the paper is to understand how a fully coupled thermo-mechanical analysis linked to a MO optimiser can lead to optimal solutions and compare it with standard approaches adopted to reduce residual stresses.

The work here presented constitutes the only research effort to date [3] addressing the direct minimisation of both process time and process-induced defects, more specifically part distortions (i.e. spring-in angle) as a result of stress build-up during cure with a multi-objective methodology. The paper tackles the cure stage of the manufacturing of the root insert for wind turbine blades by means of VARTM process and aims to achieve reduction in process time and spring-in by finding optimal cure cycles. The coupled thermo-mechanical problem associated has been solved via Finite Element (FE) solver and the solution linked to a MO Genetic Algorithm (GA) to reveal and quantify the Pareto sets of the problem where optimal designs lie. The results will be used to compare this approach with a standard approach to minimise residual stresses (i.e. overshoot temperature minimisation) and to understand how stresses leading to the spring-in are building up in the part during the different optimal cure cycles.

2. Material models

The materials used in the study are a 3AX 1800 gsm glass fibre fabric with lay-up [+45/0/-45] and the two component system Airstone™ 780E epoxy resin and 785H Hardener system [16] used by the wind industry. In Section 2.1 the chemical and thermal material models for the composite have been reported and in Section 2.2 the mechanical and thermo-mechanical models of the composite are illustrated. In Section 2.3 the coupled thermo-mechanical model is described. The heat transfer problem has been validated against different cure cycles in [15] whilst the coupled thermo-mechanical problem has been validated against the manufacturing of asymmetric laminates and reported in [17].

2.1. Chemical and thermal constitutive material models

The cure kinetics of the system follows the following behaviour [15]:

$$\frac{d\alpha}{dt} = \frac{Ae^{\left(\frac{-E}{RT}\right)}}{1 + e^{C(\alpha - \alpha_c - \alpha_T T)}} (1 - \alpha)^n \alpha^m \quad (1)$$

In the above equation A is a pre-exponential Arrhenius factor, E the activation energy of the Arrhenius function, T is the absolute temperature, R the universal gas constant, α_c , α_T , are coefficients controlling the kinetics transition from being chemically controlled to diffusion controlled, α is the degree of cure, m , n , are reaction orders for the n -th order and autocatalytic terms.

The glass transition temperature follows the Di Benedetto equation [18]:

$$T_g = T_{g0} + \frac{(T_{g\infty} - T_{g0})\lambda\alpha}{1 - (1 - \lambda)\alpha} \quad (2)$$

here $T_{g\infty}$ and T_{g0} are the glass transition temperature for the fully cured and uncured resin respectively, λ is a fitting parameter governing the convexity of the dependence on degree of cure.

The specific heat of the composite, c_p , is calculated accounting for

the contribution of fibres specific heat, c_{pf} , and resin specific heat, c_{pr} , adopting the following rule of mixture:

$$c_p = w_f c_{pf} + (1 - w_f) c_{pr} \quad (3)$$

where w_f is the weight fibre fraction. The specific heat of the fibres follows a linear dependence on temperature whilst the resin specific heat depends on temperature and degree of cure (i.e. via glass transition temperature) and are expressed as [13,15]:

$$c_{pf} = A_{f_{cp}} T + B_{f_{cp}} \quad (4)$$

$$c_{pr} = A_{rcp} T + B_{rcp} + \frac{\Delta_{rcp}}{1 + e^{C_{rcp}(T - T_g - \sigma)}} \quad (5)$$

here $A_{f_{cp}}$ and $B_{f_{cp}}$ are fitting parameters governing the linear dependence on temperature of the fibre specific heat, A_{rcp} and B_{rcp} are fitting parameters describing the temperature dependence of the uncured resin specific heat. Δ_{rcp} , C_{rcp} and σ stand for the strength, breadth and temperature shift of the step transition when vitrification occurs.

The longitudinal, K_l , and transverse, K_t , thermal conductivity of the composite is computed accounting for the thermal conductivity of the fibre, longitudinally (K_{lf}) and transversally (K_{tf}), and the resin thermal conductivity (K_r) as follows [13,15]:

$$K_{11} = v_f K_{lf} + (1 - v_f) K_r \quad (6)$$

$$K_{22} = K_{33} = v_f K_r \left(\frac{K_{lf}}{K_r} - 1 \right) + K_r \left(\frac{1}{2} - \frac{K_{tf}}{2K_r} \right) + K_r \left(\frac{K_{tf}}{K_r} - 1 \right) \sqrt{v_f^2 - v_f + \frac{\left(\frac{K_{lf}}{K_r} + 1 \right)^2}{\left(\frac{2K_{tf}}{K_r} - 2 \right)^2}} \quad (7)$$

In the case of glass fibre, the longitudinal and transverse thermal conductivities coincide. The thermal conductivity of the resin is a function of both temperature and degree of cure and is equal to:

$$K_r = a_{Kr} T \alpha^2 + b_{Kr} T \alpha + c_{Kr} T + d_{Kr} \alpha^2 + e_{Kr} \alpha + f_{Kr} \quad (8)$$

where a_{Kr} , b_{Kr} , c_{Kr} , d_{Kr} , e_{Kr} and f_{Kr} are coefficients of the polynomial function describing the resin thermal conductivity dependence on temperature and degree of cure. Table 1 reports the fitting parameters for the chemical and thermal material sub-models. The density values reported are the initial values.

2.2. Mechanical and thermo-mechanical constitutive material models

The mechanical properties of the composite namely longitudinal (E_l) and transverse (E_t) Young modulus, shear modulus (G_{12}) and in-plane Poisson ratio (ν_{12}) are described by the following equations [19]:

$$E_l = v_f E_{lf} + (1 - v_f) E_r \quad (9)$$

$$E_t = \frac{E_r}{1 - \sqrt{v_f} \left(1 - \frac{E_r}{E_{tf}} \right)} \quad (10)$$

$$G_{12} = \frac{G_r}{1 - \sqrt{v_f} \left(1 - \frac{G_r}{G_{12f}} \right)} \quad (11)$$

$$\nu_{12} = v_f \nu_{12f} + (1 - v_f) \nu_r \quad (12)$$

In the aforementioned equations v_f is the volume fibre fraction, E_{lf} , E_{tf} and E_r are the longitudinal and transverse Young modulus of the fibre and the resin modulus respectively; G_r and G_{12f} the shear modulus of the resin and fibres; ν_r and ν_{12f} the Poisson ratio of resin and fibres.

The longitudinal (a_l) and transverse (a_t) Coefficient of Thermal Expansion (CTE) of the composite and its longitudinal (γ_l) and transverse (γ_t) shrinkage are calculated in the following way [19]:

Table 1
Fitting parameters for the chemical and thermal material sub-models [15].

Cure Kinetics		
Parameters	Values	Units
A	681,085	s^{-1}
E	59,291	$J \text{ mol}^{-1}$
n	1.67	
m	0.12	
C	47.7	
α_c	0.77	
α_T	0.0016	K^{-1}
H_{tot}	434	$J \text{ g}^{-1}$
Di Benedetto		
Parameters	Values	Units
T_{go}	-55	$^{\circ}C$
$T_{g\infty}$	89	$^{\circ}C$
λ	0.476	
Specific heat		
Parameters	Values	Units
A_{fcp}	0.0014	$J \text{ g}^{-1} \text{ }^{\circ}C^{-2}$
B_{fcp}	0.841	$J \text{ g}^{-1} \text{ }^{\circ}C^{-1}$
A_{rcp}	0.0025	$J \text{ g}^{-1} \text{ }^{\circ}C^{-2}$
B_{rcp}	1.80	$J \text{ g}^{-1} \text{ }^{\circ}C^{-1}$
Δ_{rcp}	-0.25	$J \text{ g}^{-1} \text{ }^{\circ}C^{-1}$
C_{rcp}	1.10	$^{\circ}C^{-1}$
σ	16.5	$^{\circ}C$
Thermal conductivity		
Parameters	Values	Units
K_{if}	1.03	$W \text{ m}^{-1} \text{ }^{\circ}C^{-1}$
K_{rf}	1.03	$W \text{ m}^{-1} \text{ }^{\circ}C^{-1}$
a_{Kr}	0.0008	$W \text{ m}^{-1} \text{ }^{\circ}C^{-2}$
b_{Kr}	-0.0011	$W \text{ m}^{-1} \text{ }^{\circ}C^{-2}$
c_{Kr}	-0.0002	$W \text{ m}^{-1} \text{ }^{\circ}C^{-2}$
d_{Kr}	-0.0937	$W \text{ m}^{-1} \text{ }^{\circ}C^{-1}$
e_{Kr}	0.22	$W \text{ m}^{-1} \text{ }^{\circ}C^{-1}$
f_{Kr}	0.12	$W \text{ m}^{-1} \text{ }^{\circ}C^{-1}$
Density		
Parameters	Values	Units
ρ_f	2600	$kg \text{ m}^{-3}$
ρ_r	1095	$kg \text{ m}^{-3}$

$$a_l = \frac{(1 - v_f)E_r a_r + v_f E_f a_{if}}{(1 - v_f)E_r + v_f E_f} \quad (13)$$

$$a_t = (1 - v_f)a_r + v_f a_{if} + (1 - v_f)a_r v_r + v_{12f} a_{if} v_f - v_{12} a_l \quad (14)$$

$$\gamma_l = \frac{(1 - v_f)E_r \gamma_r}{(1 - v_f)E_r + v_f E_f} \quad (15)$$

$$\gamma_t = (1 - v_f)\gamma_r + (1 - v_f)\gamma_r v_r - v_{12f} \gamma_l \quad (16)$$

where γ_r and a_r are resin shrinkage and resin CTE. The mechanical and thermo-mechanical resin behaviour has been characterised and modelled in [17]. Below the model describing the evolution of resin modulus, CTE, Poisson ratio and shrinkage can be found:

$$E_r = E_{rub} + \frac{(E_{glass} + E_{glassT} * T - E_{rub})}{1 + \exp(C_m(T - T_g - \sigma_m))} \quad (17)$$

Table 2
Fitting parameters for the mechanical and thermo-mechanical material sub-models [17].

Moduli		
Parameters	Values	Units
E_{glass}	4.61 ± 0.14	GPa
E_{glassT}	-0.012	$GPa \text{ }^{\circ}C^{-1}$
E_{rub}	0.04	GPa
E_{if}	73.1	GPa
E_{rf}	73.1	GPa
G_{12f}	30	GPa
C_m	0.4	$^{\circ}C^{-1}$
σ_m	10.2	
CTE		
Parameters	Values	Units
a_{glass}	$6.0 * 10^{-5}$	$^{\circ}C^{-1}$
a_{rub}	$1.7 * 10^{-4}$	$^{\circ}C^{-1}$
a_{if}	$5.0 * 10^{-6}$	$^{\circ}C^{-1}$
a_{rf}	$5.0 * 10^{-6}$	$^{\circ}C^{-1}$
Poisson ratio		
Parameters	Values	Units
ν_{rub}	0.5	
ν_{glass}	0.35	
ν_{12f}	0.22	
Shrinkage		
Parameters	Values	Units
γ_α	0.019	

$$a_r = a_{rub} + \frac{(a_{glass} - a_{rub})}{1 + \exp(C_m(T - T_g - \sigma_m))} \quad (18)$$

$$\nu_r = \nu_{rub} + \frac{(\nu_{glass} - \nu_{rub})}{1 + \exp(C_m(T - T_g - \sigma_m))} \quad (19)$$

$$\gamma_r = \gamma_\alpha \alpha \quad (20)$$

In the equations above E_{rub} and E_{glass} represent the resin modulus at rubbery and glassy state, E_{glassT} governs the dependence on temperature of the resin modulus at the glassy state, a_{rub} and a_{glass} are the resin CTE at rubbery and glassy state respectively, ν_{rub} and ν_{glass} are the resin Poisson ratio at rubbery and glassy state; C_m and σ_m are fitting parameters governing the mechanical glass transition whilst γ_α is the maximum linear resin shrinkage. Table 2 reports the fitting parameters for the mechanical and thermo-mechanical material sub-models.

2.3. Coupled thermo-mechanical model

The coupled thermo-mechanical problem has been set up on the FE solver Marc.Mentat® [20]. The elements used for the simulation are three-dimensional isoparametric 8-nodes brick composite for coupled thermo-mechanical analysis (Marc® element type 149) [21]. Material properties and boundary conditions are implemented using user sub-routines [22]. The FE model is representative of the cure stage of the manufacturing of the root insert by means of VARTM process. Fig. 1 a) depicts a drawing of the root insert geometry and boundary conditions application. Due to symmetry reasons only half of the root insert is considered. The model consists of 3780 elements and 5952 nodes. A strip of the root insert at its thickest segment (i.e. the most challenging region in terms of curing) has been modelled (see Fig. 1 b)) therefore zero heat flux has been applied in x direction. Displacements and rotation boundary conditions have been applied to avoid rigid body

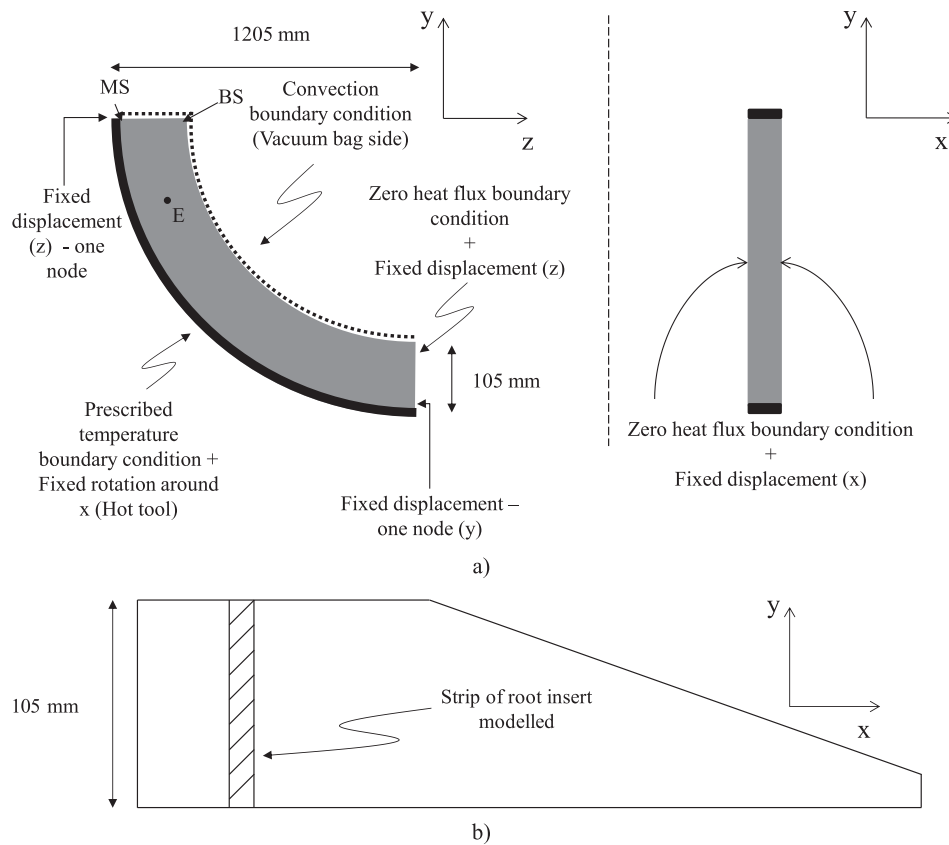


Fig. 1. a) Schematic of the model geometry showing the Mould Side (MS) and vacuum Bag Side (BS) node locations and boundary conditions application b) Root insert thickness along x.

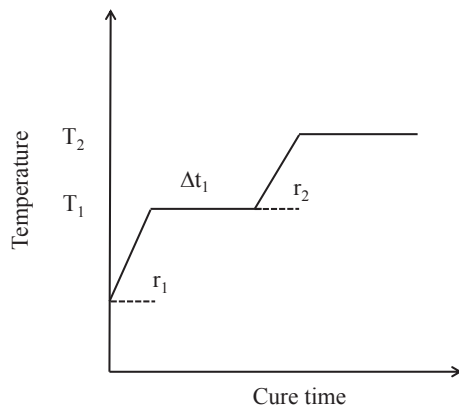


Fig. 2. Parameterised cure profile.

movement. At the end of the cool-down the part is left free to deform. To model the heat exchange by convection occurring at the vacuum bag side, natural air convection boundary condition is applied via UFILM user subroutine. The ambient temperature considered for the air is 25 °C whilst the heat transfer coefficient is equal to 13.6 W/m² °C [23]. Fixed temperature boundary condition following the cure profile is applied to nodes in contact with the hot tool via FORCDT user subroutine. The cure cycle of the infused part, as parameterised in Fig. 2, starts at the end of the infusion. Initial temperature condition equal to ambient temperature is applied to all the nodes in the model. The infusion time for such a part has been calculated by Darcy's law and considering the infusion from both top and bottom sides. The infusion time was found to be 116 min. The infusion occurs at room temperature, therefore using the cure kinetics model it is possible to calculate the initial degree of cure for the cure stage which is 0.14. Cure kinetics,

specific heat and thermal conductivity models have been implemented using UCURE, USPCHT and ANKOND respectively while HOOKLW, ANEXP have been used to implement modulus, Poisson and CTE models. The model for shrinkage has been implemented using user defined tables.

3. Multi-objective optimisation methodology

Two multi-objective optimisation problems have been designed. The first targets the minimisation of process time ($t_{process}$) and spring-in (θ) by identifying optimal cure cycles. The second targets the minimisation of process time and maximum overshoot temperature (ΔT_{max}) by finding optimal cure cycles. The goal of the second optimisation is to investigate the correlation between minimisation of overshoot temperature on spring-in. The MRCC for the resin system under study imposes a one dwell profile at 70 °C [16]. An existing Genetic Algorithm (GA) capable of addressing multi-objective optimisation problems that has been tested against different benchmarks problems [24] and that proved its flexibility to couple with different commercial FE solvers, has been adapted to tackle the problem at hand. The curing problem has been shown to be riddled by local minima [13] therefore an evolutionary algorithm had to be used since gradient based techniques are likely to get stuck in one of these local minima. The GA used has combined metric that penalises dominated individuals and individuals closer to each other than a threshold distance. The details of the GA together with reliability, reproducibility, robustness and performance tests against standard benchmarks problems are reported in [24]. The cure cycles are sought amongst two-dwell cycles therefore, five design parameters have been identified to parametrically describe the cure cycle: temperature of first and second dwell (T_1 , T_2), first dwell duration (Δt_1), ramp rate to the first dwell (r_1) and to the second dwell (r_2); the duration of the second dwell is not considered as a parameter since it is

Table 3
Design parameter ranges.

Parameters	Ranges	Units
T_1	30–70	°C
T_2	70–105	°C
Δt	2–240	min
r_1	0.1–4.0	°Cmin ⁻¹
r_2	0.1–4.0	°Cmin ⁻¹

Table 4
Optimisation parameters.

GA input	Values
Max number of generations	10
Individuals per population	30
Individuals per reproduction	24
Elite individuals	4
Size of Pareto set	30
Mutation probability	0.005
Cross-over probability	0.5

considered as the necessary time to reach in the model a minimum degree of cure of 90% amongst all elements. A schematic of the parameterised cure profile is presented in Fig. 2. The 90% threshold has been selected as this is the minimum degree of cure achieved within the model when MRCC is applied. From this point a fixed cool-down rate to room temperature at 0.5 °C/min is applied. The cool-down has been kept out of the optimisation parameters to keep the focus on the stresses generated whilst the part is curing. The final process time takes the cool-down time into account. Each parameter of the optimisation is assigned a range of possible values. The ranges are reported in Table 3 and have been chosen considering technological limits and possibilities of the moulds used by the wind blades manufacturer. Table 4 reports the optimisation parameter values which are tuned for the root-insert problem solution considering previous optimisation problems [15].

The GA and the FE solver Marc.Mentat communicate via a user defined interface that takes care of updating the input file of the simulation with the new design parameters sets dictated by the GA. The new simulation is then run by the interface. The relevant outputs (i.e. the objectives of the optimisation) are identified via user subroutines defined in Marc.Mentat (i.e. UPSTNO, UEDINC) and written by the interface in temporary text files. The values are then read by the interface and sent to the GA which performs the dominance routine for the build-up of the Pareto sets. The GA converges to a final Pareto front once no further improvements are detected. Fig. 3 sketches a schematic representing the main interactions between GA, interface and FE solver Marc.Mentat. In the present work, the optimisation and corresponding Pareto front, where the objectives are process time ($t_{process}$) and spring-in (θ) which is calculated from the displacement in z direction, will be referred to as “thermo-mechanical”. Fig. 4 illustrates a graphical definition of the spring-in (θ). The second optimisation, where the objectives are process time ($t_{process}$) and maximum overshoot temperature (ΔT_{max}), will be named “thermal”.

4. Results

4.1. Thermo-mechanical optimisation

In Fig. 5 the results from the optimisation are reported (i.e. thermo-mechanical Pareto front). The Pareto front shows a linear relationship between the two objectives. The set of optimal solutions span from 245 min and 325 min in terms of process time and from 0.13° to 0.7° with respect to spring-in, which corresponds respectively to 2 mm and 13 mm in terms of maximum displacement in z direction (see Fig. 3). A designer can select one of these trade-off points according to the end

application and requirements. A single simulation of the coupled thermo-mechanical problem takes approximately 20 mins on a standard desktop equipped with a 3.5 GHz CPU. According to the optimisation parameters there are 30 individuals per population and 10 generation to reach convergence therefore a total of 300 simulations are performed. The optimisation takes around 100 h (i.e. four days) to complete. The MRCC solution provided a component with 0.52° spring-in and 400 mins process time. Applying solutions belonging to the Pareto front can bring reductions up to 32% in process time and up to 75% in spring-in compared to MRCC solution. The result points out that MRCC does not provide an appropriate thermal profile for the root insert under study.

The two individuals at the edge of the Pareto (A, C) have been chosen to provide a wide variety in design parameters, therefore the extreme individuals in the Pareto (i.e. shortest/longest process time and biggest/smallest spring-in) plus one located in between (B) in the objective space (see Fig. 4). Table 5 reports the design parameters of these three individuals (i.e. solutions). In the table, the maximum overshoot temperature compared to the mould temperature (i.e. ΔT) is also reported. The temperature of the first dwell is similar for the three individuals. However, the duration of the first dwell is the longest for individual A and the shortest for individual C. This means that individual A will near the ramp to second dwell with a more developed reaction and therefore less prompt to exothermic phenomena during the switch to the second dwell temperature. Additionally, the second dwell temperature decreases from individual A to C. Individual C also has the highest overshoot temperature which combined with the lowest second dwell temperature results in the larger temperature gradient through thickness and consequently poorer quality and larger spring-in compared to the other solutions. The selection of the fast second ramp rate aims at minimising the gap with the temperature increase due to exothermic reaction. The relationship between the overshoot temperatures and spring-in angles from the solutions of the thermo-mechanical Pareto front has been shown in Fig. 6. A linear relationship between overshoot temperature and spring-in of the part holds for the case under study, which seems in line with the often seen trends in literature to minimise overshoot temperature in order to reduce residual stresses [6,13,25,26]. It was assumed in these papers that the higher the overshoot temperature in the cure cycles was, the larger the residual stresses induced in the part would be.

In Fig. 7 the evolution of temperature profile for a node at the boundary condition and a node at the location that experiences the highest exothermic reaction (i.e. location E in Fig. 1), has been plotted for individuals A and C. The two individuals share the same first dwell temperature therefore it is easier to understand how the optimisation deals with the two competitive objectives. In the case of A, the cure profile dictates a first dwell duration of 101 min. This allows the reaction to start mildly, and once it kicks in switching quickly to the second dwell temperature so to contain the thermal gradient through thickness. Individual A privileges reducing the spring-in over process time. For individual C, the second dwell temperature is reached within 50 min with the temperature at location E lagging behind by about 50 °C. This is the primary cause of a quick exothermic build up since the resin at this location still stores the majority of its chemical potential and gets activated at high temperature (i.e. 92 °C). Individual C prioritises process time over spring-in. Although counter-intuitive, the results show that lowering the second dwell temperature leads to worse quality performance, this is due to the fact that such a choice causes a greater temperature gradient between the region close to the mould and the region where exotherm occurs.

4.2. Thermal Pareto vs Thermo-mechanical Pareto

In Fig. 8 the results from the optimisation analysis applied to only the heat transfer problem (i.e. Thermal Pareto) are reported together with the thermo-mechanical Pareto front. Optimisation analysis based

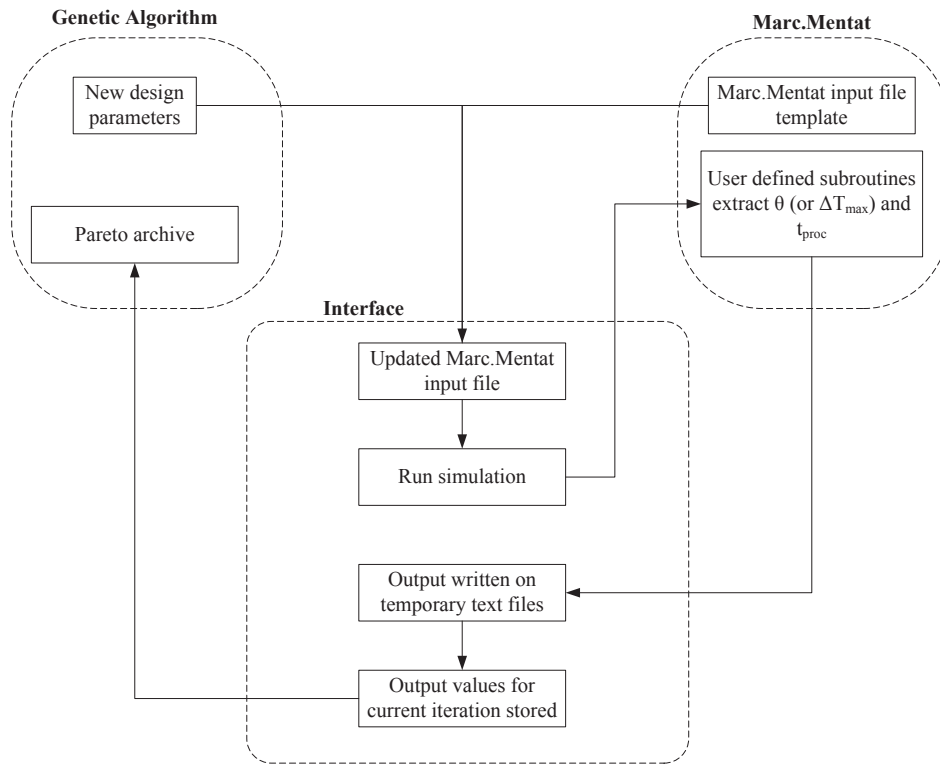


Fig. 3. Interface functioning.

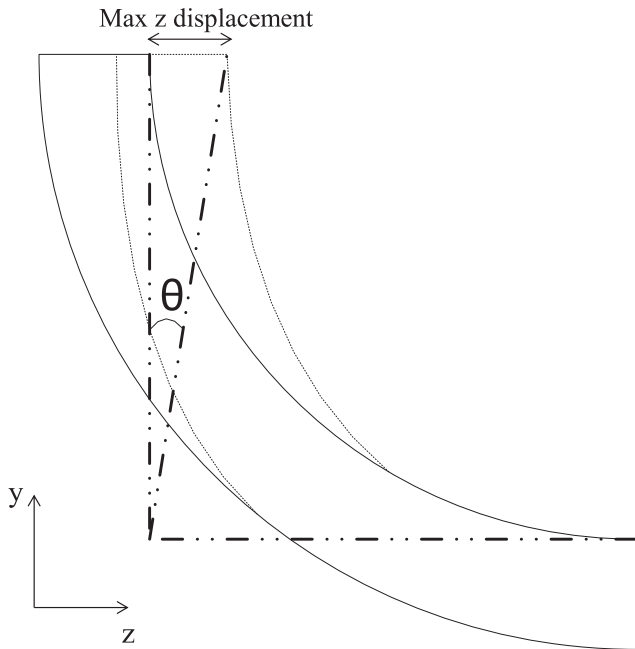


Fig. 4. Geometrical definition of θ .

on the solution of solely heat transfer problems achieves convergence after ten generations and takes about 40 h to complete. Therefore, there is 60% less computational time than the optimisation of the thermo-mechanical problem. In terms of process time, the Thermal Pareto spans from 235 min to 305 min, which is shorter than the solutions found by the Thermo-mechanical Pareto. However, as reported in Table 6, the corresponding minimum spring-in achieved by individual A' is of 0.31° (i.e. 6 mm max displacement) which is 60% larger than the one obtained by individual A. The same applies for individual C' which ends up in a final spring-in of 0.83° (i.e. 16 mm max displacement) compared

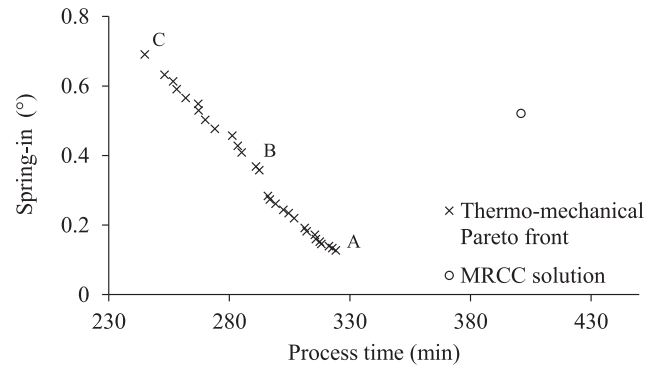


Fig. 5. Pareto optimal solutions vs MRCC solution.

to the 0.70° (i.e. 13 mm max displacement) of individual C. The objective space of both Pareto fronts shows a linear dependence of the quality related objective (i.e. spring-in/overshoot temperature) with process time. Approximately 20°C increase in overshoot temperature generates a 0.3° increase in spring-in which is the same trend observed in Fig. 6. From the analysis of the design parameters reported in Table 6 it can be observed that second dwell temperature and first dwell duration follow the same trend as in Table 5. However, the first dwell temperatures and first ramp rate tend to be higher with respect to the individuals in the thermo-mechanical Pareto front. Consequently, although the result is optimal in terms of overshoot temperature, it does not directly translate into an optimal result in the spring-in. This is because the generation of residual stresses is a complex phenomenon and overshoot temperature is only one aspect that contributes to it. Therefore, minimisation of overshoot temperature can be seen as an effective tool to reduce residual stresses formation and deformation such as the spring-in, however, it does not necessarily lead to the most efficient front. This is proven by the fact that when spring-in is treated as direct objective, the thermo-mechanical Pareto front unveils solutions with only 0.13° deflection that were not detected by only the

Table 5
Design parameters of three individuals belonging to the Thermo-mechanical Pareto front.

Selected individuals	Design parameters							
	T_1 (°C)	T_2 (°C)	Δt (min)	r_1 (°C min ⁻¹)	r_2 (°C min ⁻¹)	θ (°)	t_{proc} (min)	ΔT (°C)
A	33.2	104.8	101	3.32	3.85	0.13	324	41
B	38.3	103.7	56	1.48	2.40	0.37	291	50
C	33.2	92.2	34	1.48	4.00	0.70	245	72

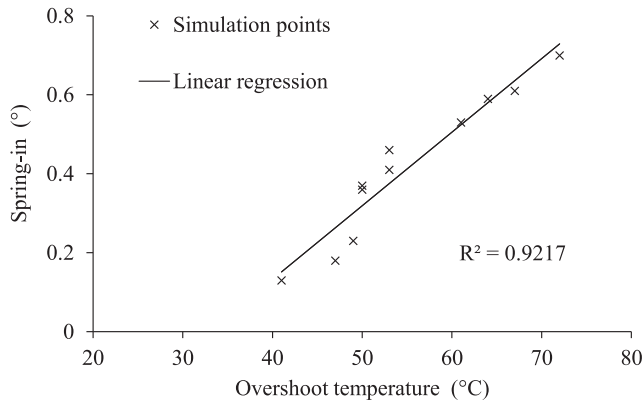


Fig. 6. Relationship between spring-in and overshoot temperature.

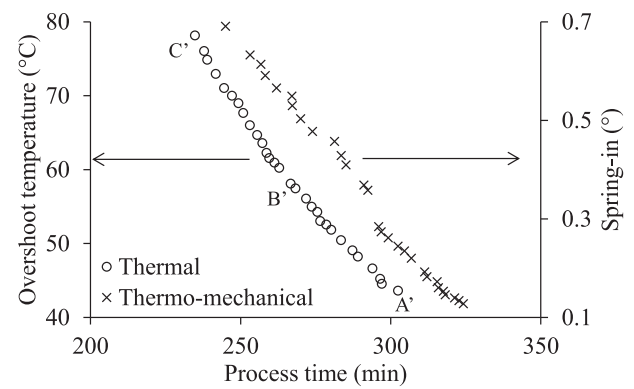


Fig. 8. Thermal Pareto vs Thermo-mechanical Pareto.

thermal analysis.

In the light of this result, the optimisation of only the heat transfer problem has the advantage to require 60% less computational time, and less material characterisation campaigns to perform (i.e. only cure kinetics, specific heat and thermal conductivity are needed). Nevertheless, it has the disadvantage that better solutions might hide behind. Consequently, a more explicit definition of the quality related objective (i.e. spring-in) can lead to solutions that would remain hidden otherwise.

4.3. Transverse stresses development during curing

To understand how stresses leading to the spring-in are building up in the part during the different optimal cure cycles, the details of the stress evolution associated with individuals A and C (see Fig. 5) will be studied in this section. It is of interest to follow the stress evolution within the part and compare it with the glass transition temperature evolution and resin modulus development. This analysis has proved meaningful in a previous work, clarifying certain aspects of residual stresses formation [17]. For each individual, two candidate nodes, one at the vacuum bag side (BS) and one at the mould side (MS) have been selected. Node locations are shown in Fig. 1. In Fig. 9 the results of MS node of individual A, are illustrated. Fig. 9 a) presents the temperature evolution and corresponding glass transition temperature development.

The MS node follows exactly the cure profile assigned since a temperature boundary condition is applied. Gelation at this node begins at about 164 min and vitrification ends at about 245 min. Fig. 9 b) presents the resin modulus evolution and transverse stress development which play significant role in the spring-in formation. As the resin modulus increases (i.e. gelation), compressive stress starts building up (1 MPa). The increase in resin modulus was observed in previous work to start when the difference between the temperature of the part and its glass transition temperature was about 25 °C (defined as start of gelation in this paper) [17]. The vitrification process ends when $T = T_g$. The stresses in Fig. 9 b) are compressive in nature at the early stage of the gelation process since the part is in the cooling stage, here the transverse CTE is dominant causing the generation of compressive stresses within the part. As the resin modulus keeps increasing, the resin becomes able to carry and transfer load between plies. Together with the mismatch in CTE of the $\pm 45^\circ$ and 0° plies, this leads to the following behaviour: the $\pm 45^\circ$ plies starts dominating the 0° ply in transverse direction. The $\pm 45^\circ$ plies contract more in transverse direction (CTE of composite is larger in this direction) therefore they expand in longitudinal direction and stretch the 0° ply transversally ending up in tensile stresses in the 0° layers. The change in the slope of the residual stress development from about 164 min to about 240 min is due to the glass transition and the consequent change in CTE values [17]. Once vitrification is completed, the stresses develop linearly with cooling rate. At the MS node the final tensile stress developed at the end

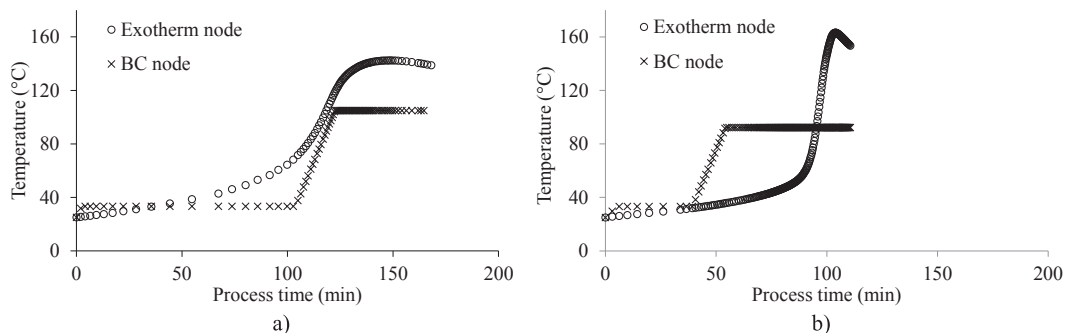


Fig. 7. Temperature evolution comparison between individual A (left side) and C (right side) at location E (Fig. 1) where exotherm occurs.

Table 6
Design parameters of three individuals belonging to the Thermal Pareto front.

Selected individuals	Design parameters							
	T_1 (°C)	T_2 (°C)	Δt (min)	r_1 (°C min ⁻¹)	r_2 (°C min ⁻¹)	θ (°)	t_{proc} (min)	ΔT (°C)
A'	42.7	102.3	53	0.44	3.11	0.31	302	44
B'	43.3	93.3	53	2.40	1.17	0.52	267	58
C'	68.5	93.5	49	2.43	3.14	0.83	235	78

of the process is of 9.3 MPa.

In Fig. 10 the details of BS node of individual A, are illustrated. Fig. 10 a) presents the temperature evolution and corresponding glass transition temperature development. The BS node initially shows a higher cooling rate (-1.5 °C/min) compared to the MS node (-0.5 °C/min) since it is located where natural convection boundary condition is applied. Fig. 10 b) depicts the resin modulus evolution and transverse stress development. Gelation at this node begins at about 160 min and vitrification completes at about 216 min. The cooling rate at the end of the vitrification is about -0.6 °C/min, comparable with MS node, explaining the similar level of compressive stress developed. However, at the beginning of the cool-down the MS node has reached its final degree of cure (i.e. 95%) whilst the BS node is at 84%. Therefore, at the moment when $T = T_g$, MS node has 1.3 MPa residual stresses whilst BS node 0.7 MPa. From this point onward the evolution of stresses mirrors the cooling rate. The MS node develops higher residual stresses at the end of the cool-down (about 9 MPa) compared to the BS node (about 7 MPa).

In Fig. 11 the results of MS node of individual C, are displayed. Fig. 11 a) shows the temperature evolution and corresponding glass transition temperature development. The MS node follows the cure profile applied and hence the cooling rate is -0.5 °C/min. Gelation at this node begins at about 100 min and vitrification completes at about 167 min. From the observation of Fig. 11 b) similar conclusions to individual A can be drawn. It is of interest to notice that in this case the stress build-up starts with very small tensile stress development during the second dwell (shrinkage dominated). The cure profile adopted leads to the generation of less compressive stress (0.5 MPa) compared to individual A. Since the two nodes have the same cooling rate, the smaller amount of compressive stress generated in this case, to higher final tensile stress state (10.3 MPa) compared to MS node of individual A (9.3 MPa).

Fig. 12 reports the details of BS node for individual C. In Fig. 12 a) the temperature history at the node together with the glass transition temperature evolution is depicted. Gelation at this location begins at about 116 min and vitrification finishes at about 190 min. The location experiences a sharp exothermic reaction and consequently a high cooling rate after the peak (-6.5 °C/min) compared to the MS node. In the proximity of $T = T_g$ the cooling rate is -1.2 °C/min. The higher cooling rate generates higher compressive stress development (1.5 MPa) compared to individual A. Furthermore, the cooling rate after

vitrification is about -0.23 °C/min which is lower than the MS node. The combination of these two effects leads to a milder final tensile stress of about 5.5 MPa. The development of stress and resin modulus for the current node are shown in Fig. 12 b). Comparing the stress developed by individual A and C at the end of the respective cure cycles it can be noticed that the final difference between the mould side and bag side stresses are of 2 MPa for individual A and 5 MPa for individual C, explaining the development of a greater spring-in for individual C. Furthermore, the two individuals result in the same degree of cure difference through thickness (i.e. 0.04) being 0.95–0.91 for individual A and 0.93–0.97 for individual C. The detailed analysis of the stress evolutions of the individuals selected points out that it is possible to engineer different level of residual stresses within a part and use it to improve part quality by designing appropriate cure cycles. Furthermore, for the case study at hand it showed that higher cooling rate after gelation but before completion of vitrification are beneficial since they introduce compressive stresses that counteract the final tensile stress state. However, once vitrification is completed opposite behaviour is shown and slower cooling rate leads to less formation of residual stresses.

5. Conclusions

The multi-objective optimisation study developed in the present paper constitutes the first study on direct optimisation of process time and spring-in angle (as a measure of quality of the final product). It was applied on an ultra-thick composite structure, representing half of the circular root insert of a wind turbine blade. The paper highlights that, a thermal model only, which uses the minimisation of overshoot temperature within the composite part as the typically used quality objective can be a metric to reduce residual stresses and part deformation but might not lead to optimal solutions. It is shown that similar process times are obtained however the minimum spring-in achieved is larger. In the case study, it was shown that minimising the spring-in rather than the overshoot temperature can lead to additional 60% spring-in reduction. The thermo-mechanical Pareto front, obtained when the GA optimiser was linked with a coupled thermo-mechanical analysis, allows for reduction in process time of about 32% and 75% reduction in spring-in compared to MRCC solution. The Pareto front finds optimal solutions in terms of process time and part quality; within the set of solutions the designers can choose the cure cycle that satisfies their

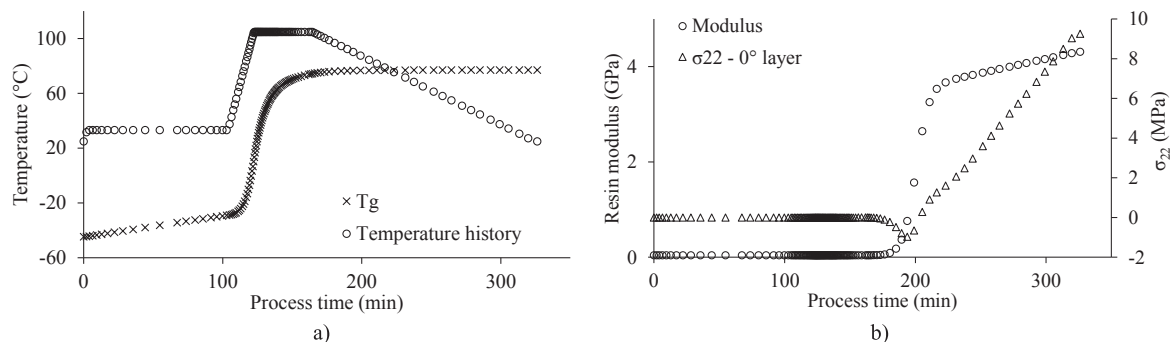


Fig. 9. Details of the mould side node for individual A a) Tg evolution and temperature history b) Resin modulus development and transverse stress.

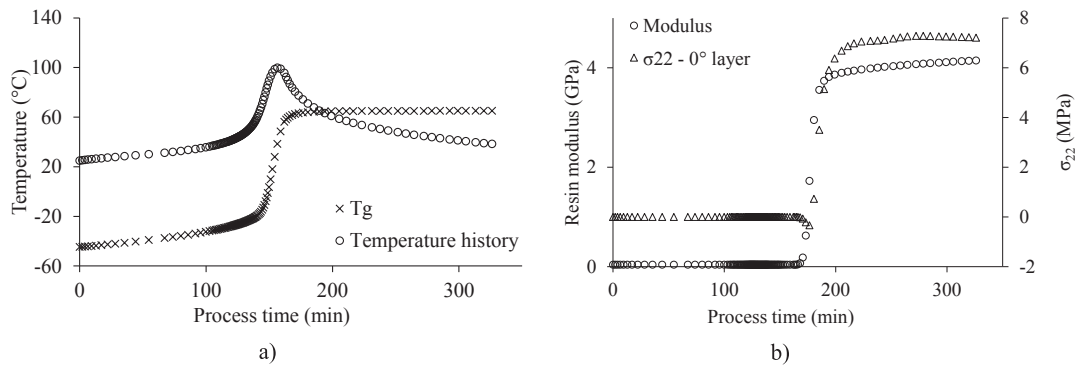


Fig. 10. Details of the bag side node for individual A a) Tg evolution and temperature history b) Resin modulus development and transverse stress.

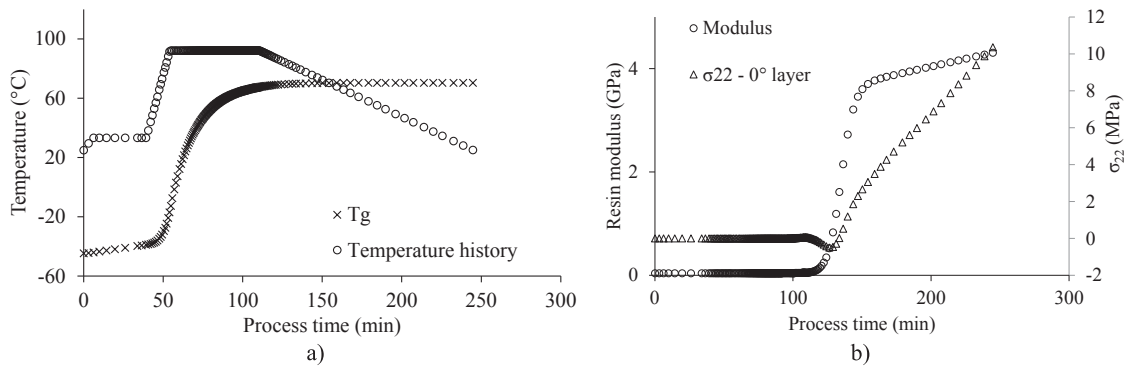


Fig. 11. Details of the mould side node for individual C a) Tg evolution and temperature history b) Resin modulus development and transverse stress.

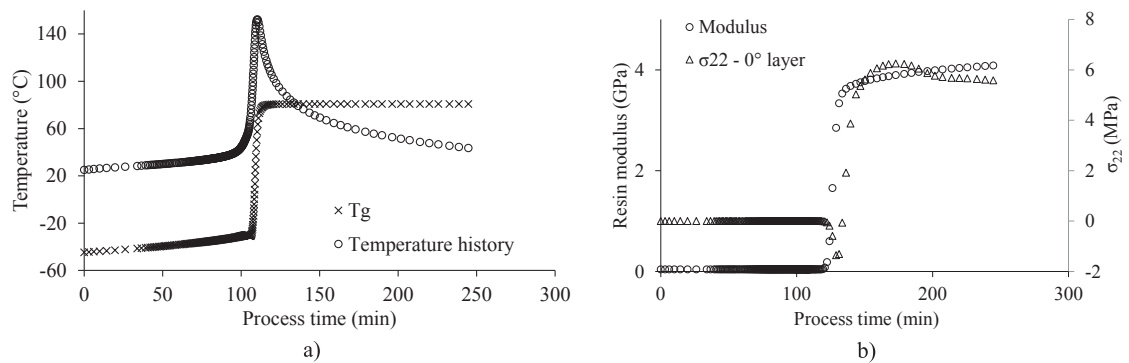


Fig. 12. Details of the bag side node for individual C a) Tg evolution and temperature history b) Resin modulus development and transverse stress.

needs (i.e. solution C which has the shortest process time and lowest second dwell temperature is an ideal candidate to reduce the carbon footprint of the process).

The thermal Pareto front achieves 35% process time reduction and 38% spring-in reduction compared to the MRCC, and is obtained using 60% less computational time compared to the thermo-mechanical Pareto front. This suggests that optimisation of only the heat transfer problem with overshoot temperature as quality related objective could be used in areas where dimensional tolerances are less stringent whilst a coupled thermo-mechanical analysis is required in areas where this is crucial such as aerospace and wind industry.

The analysis of the transverse residual stresses brings up the importance of cure cycle design to optimise the stress evolution to minimise the final spring-in. Given the thickness at play it is important to generate a similar amount of residual stresses through the thickness (i.e. minimum difference between outer and inner side). This can be achieved by designing cure cycles which enables small gradients through thickness of temperature, glass transition temperature and degree of cure. The final stress state in the part is tensile in nature

which is due to the presence of the $\pm 45^\circ$ layers in the lay-up used in this study. However during the cure cycle there is generation of compressive stresses that can lower the final tensile state of the part. Optimal cure cycle design must engineer compressive stresses after gelation but before completion of vitrification to successfully counteract the generation of tensile stresses after. Also, after vitrification is completed, the lower the cooling rate the less the residual stresses generated. Therefore, the present study suggests that two cooling rates should be designed one before and one after vitrification.

Undertaking an optimisation analysis based on a coupled thermo-mechanical model for each component to be manufactured can bring significant benefits in terms of process time/cost and tolerances compliance. The methodology presented can be used to identify optimal solutions to minimise process time and maximise part quality.

CRediT authorship contribution statement

G. Struzziero: Conceptualization, Data curation, Formal analysis, Investigation, Methodology, Validation, Writing - original draft. **J.J.E.**

Teuwen: Funding acquisition, Project administration, Resources, Supervision, Writing - review & editing.

Declaration of Competing Interest

The authors declare that they have no known competing financial interests or personal relationships that could have appeared to influence the work reported in this paper.

Acknowledgments

This work was supported by ADEM innovation lab, A green Deal in Energy Materials of the Ministry of Economic Affairs of the Netherlands (www.adem-innovationlab.nl). Data underlying this research are available through the repository of the Dutch Universities of Technology, <http://researchdata.4tu.nl/home>, with <https://doi.org/10.4121/uuid:9fb922cb-8959-421d-ac22-a4717cfa7e22>.

References

- [1] Ibbotson S, Kara S. LCA case study. Part 1: cradle-to-grave environmental footprint analysis of composites and stainless steel I-beams. *Int J Life Cycle Assess* 2013;18(1):208–17.
- [2] Xie J-b, Fu J-x, Liu S-y, Hwang W-s. Assessments of carbon footprint and energy analysis of three wind farms. *J Cleaner Prod* 2020;254:120159.
- [3] Struzziero G, Teuwen JJE, Skordos AA. Numerical optimisation of thermoset composites manufacturing processes: A review. *Compos A Appl Sci Manuf* 2019;124:105499.
- [4] Pillai VK, Beris AN, Dhurjati PS. Implementation of model-based optimal temperature profiles for autoclave curing of composites using a knowledge-based system. *Ind Eng Chem Res* 1994;33(10):2443–52.
- [5] Pillai VK, Beris AN, Dhurjati PS. Heuristics guided optimization of a batch autoclave curing process. *Comput Chem Eng* 1996;20(3):275–94.
- [6] Bailleul JL, Sobotka V, Delaunay D, Jarny Y. Inverse algorithm for optimal processing of composite materials. *Compos A Appl Sci Manuf* 2003;34(8):695–708.
- [7] Gopal AK, Adali S, Verijenko VE. Optimal temperature profiles for minimum residual stress in the cure process of polymer composites. *Compos Struct* 2000;48(1):99–106.
- [8] Kam TY, Lai FM, Sher HF. Optimal parameterers for curing graphite/epoxy composite laminates. *J Mater Process Tech* 1995;48(1–4):357–63.
- [9] White SR, Hahn HT. Cure cycle optimization for the reduction of processing-induced residual stresses in composite materials. *J Compos Mater* 1993;27(14):1352–78.
- [10] Zhu Q, Geubelle PH. Dimensional accuracy of thermoset composites: Shape optimization. *J Compos Mater* 2002;36(6):647–72.
- [11] Ruiz E, Trochu F. Comprehensive thermal optimization of liquid composite molding to reduce cycle time and processing stresses. *Polym Compos* 2005;26(2):209–30.
- [12] Ruiz E, Trochu F. Multi-criteria thermal optimization in liquid composite molding to reduce processing stresses and cycle time. *Compos Part A: Appl Sci Manuf* 2006;37(6 SPEC. ISS.):913–24.
- [13] Struzziero G, Skordos AA. Multi-objective optimisation of the cure of thick components. *Compos A Appl Sci Manuf* 2017;93:126–36.
- [14] Matsuzaki R, Yokoyama R, Kobara T, Tachikawa T. Multi-objective curing optimization of carbon fiber composite materials using data assimilation and localized heating. *Compos A Appl Sci Manuf* 2019;119:61–72.
- [15] Struzziero G, Teuwen JJE. Effect of convection coefficient and thickness on optimal cure cycles for the manufacturing of wind turbine components using VARTM. *Compos A Appl Sci Manuf* 2019;123:25–36.
- [16] Airstone™ Infusion System Product. <http://www.dowepoxysystems.com>.
- [17] Struzziero G, Nardi D, Sinke J, Teuwen JJE. Cure-induced residual stresses for warpage reduction in thermoset laminates. *J Compos Mater* 2020.
- [18] Pascault JP, Williams RJJ. Relationships between glass transition temperature and conversion. *Polym Bull* 1990;24(1):115–21.
- [19] Mesogitis TS, Skordos AA, Long AC. Stochastic simulation of the influence of fibre path variability on the formation of residual stress and shape distortion. *Polym Compos* 2017;38(12):2642–52.
- [20] Marc® volume A: Theory and user information. <http://www.mssoftware.com>; 2015.
- [21] Marc® volume B: Element library. <http://www.mssoftware.com>; 2015.
- [22] Marc® volume D: User subroutines and special routines. <http://www.mssoftware.com>; 2015.
- [23] Mesogitis TS, Skordos AA, Long AC. Stochastic heat transfer simulation of the cure of advanced composites. *J Compos Mater* 2015;50(21):2971–86.
- [24] Struzziero G. Optimisation of the VARTM process. PhD thesis; 2014.
- [25] Antonucci V, Giordano M, Hsiao K-T, Advani SG. A methodology to reduce thermal gradients due to the exothermic reactions in composites processing. *Int J Heat Mass Transf* 2002;45(8):1675–84.
- [26] Jahromi PE, Shojaei A, Reza Pishvaie SM. Prediction and optimization of cure cycle of thick fiber-reinforced composite parts using dynamic artificial neural networks. *J Reinf Plast Compos* 2012;31(18):1201–15.